APPLICATION OF A NEW INVERSE METHOD TO NONDESTRUCTIVE EVALUATION

N. Bleistein and J. K. Cohen
University of Denver
Denver, Colorado

ABSTRACT

When a wave impinges upon an irregularity in an otherwise homogeneous medium, the wave is deformed in a manner which is characteristic of the irregularity. This is the basis of a method of nondestructive evaluation of materials. Problems in which one seeks information about material properties from scattered waves are known as inverse problems. Traditionally, such problems are analyzed either by cataloging many solutions of direct problems and comparing the results of a given experiment with catalogs, or by attempting to solve the relevant equation of wave properties backwards in time. In contrast, we formulate the inverse problem as an equation or system of equations in which one of the unknowns is a function which directly characterizes the irregularity to be determined. Under the assumption of small sized anomalies or small changes in media properties, our system reduces to a single linear integral equation for this "characteristic" function. In many cases of practical interest, this equation admits closed form solutions. Even under the constraints of practical limitations on the data, information about the irregularity can be deduced. As an example, we consider the case of a void in a solid probed by acoustic waves. We show how high frequency data can be directly processed to yield the actual shape of the anomaly in a region of the surface covered by specular reflection of the probe. In the low frequency case, we show how to directly process the data to yield the volume, centroid, and "products of inertia" of the void.

Introduction

The application of a new inverse method to non-destructive evaluation is described. In particular, detection of a small hole in an otherwise homogeneous solid is discussed. The scattering of an acoustic probe by the hole is considered. It is shown that the scattered wave is proportional to the Fourier transform of the characteristic function of the domain occupied by the hole. The characteristic function is equal to unity in that domain, and zero outside. Thus, knowledge of this function characterizes the domain. The basic result is derived under the assumption that the scatterer is small - allowing use of the Born approximation - and "far" from the surface of the solid. Some features of aperture limited - band limited and aspect angle limited - observations are discussed. The applicability of this inverse method to non-destructive evaluation is demonstrated by this preliminary analysis.

When a wave (e.g., acoustic, elastic, electromagnetic) propagates through a medium, the wave is deformed by irregularities in that medium. The deformation of the probing wave is characteristic of the irregularity. This is the basis of a method for non-destructive evaluation of solid materials. A known probing wave is introduced into the medium. The wave "scattered" by the irregularity is observed. The nature of the irregularity is to be inferred from the nature of the scattered wave.

The type of problem we have described here is called an inverse problem. The corresponding direct problem would be to find the scattered wave given the "incident wave" (probe) and the irregularities of the medium. Inverse problems are often attacked indirectly; i.e., one solves direct problems for prescribed irregularities, seeking an irregularity for which the scattered wave most nearly approximates the data.

In contrast, we are engaged in research on direct solutions of the inverse problem. That is, we formulate an equation or system in which the solution is a function (or functions) which directly characterizes the "unknown" of the inverse problem. Recently, we have examined the non-destructive evaluation problem from the point of view of our inverse methods. Our conclusion is that our methods are most definitely applicable to this problem. The objective of this report is to describe our preliminary analysis.

Our basic model is as follows. We suppose that there is a small convex hole in an otherwise homogeneous solid. The size and shape of the hole are to be determined from observations of scattered waves on the surface of the solid. The waves are produced by acoustic sources on the surface.

We assume that the hole size is small compared to the distance to the boundary. This allows us to linearize an essentially non-linear problem. This linearization is equivalent to the Born approximation, Morse & Feshback.[8] Further exploitation of this scaling assumption allows us to reduce the inverse problem to a statement about the Fourier transform of the characteristic function of the region of the hole. The characteristic function is equal to unity inside the hole and equal to zero outside. Thus, knowledge of this function describes the hole.

In any practical problem, observations cannot be made over "all" frequencies, or over all directions of scatter. However, the vector variable in the Fourier transform introduced above has magnitude proportional to frequency and direction related to the source and receiver locations. Consequently, one must next examine the problem of extracting information about the characteristic function from its aperture limited - band

limited and aspect angle limited - Fourier transform. We discuss the low frequency and high frequency limits separately in the sections on "Low Frequency Analysis of the Characteristic Function" and "High Frequency Analysis."

Preliminary discussions focused on the low frequency limit only. However, analysis of magnitudes provided to us suggest that the high frequency limit might be exploited as well. To see why this is so, we note that the relevant parameter for high frequency approximation is:

$$\Lambda = 2\pi fa/c \quad , \tag{1}$$

where f is frequency in Hertz, "a" is a typical length, and c is soundspeed. Values provided to us were a maximum frequency of 8×10^6 Hz, a length scale of 50 mils, and a soundspeed of 21,000 ft/sec, for which $\Lambda = 10$. From the discussion of "High Frequency Analysis" it will become clear that such a value of Λ will produce "tolerable" results, while an increase in Λ by a factor of two will produce good results, and an increase by a factor of three will produce excellent results.

The advantage of high frequency data is that it can be used to produce a "picture" of the actual flaw. On the other hand, we show that from low frequency data we can find the volume, center of mass, and dimensions and orientation of an "equivalent" ellipsoid. Equivalence in this context means that the ellipsoid has the same centroid and mass-normalized products of inertia as the flaw to be detected. Orientation is then deduced by "diagonalizing" the matrix of products of inertia.

Basic Formulation

The mathematical formulation of the problem will be described with the aid of Fig. 1. A hole occupies a region D bounded by a surface S inside an otherwise homogeneous region A. The total field, inside the region D-A is assumed to satisfy the Helmholtz equation:

$$(\nabla^2 + \omega^2/c^2)U = 0 \quad . \tag{2}$$

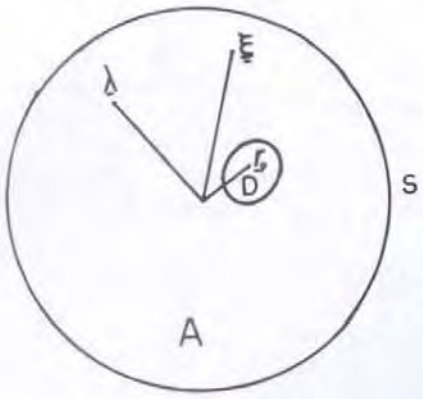

Figure 1. Basic model for analysis.

Here, ∇^2 denotes the Laplacian in three dimensions, ω is the frequency in radians/second, and c is the soundspeed. An impulsive source is located at $\underline{\lambda} = (\lambda_1, \lambda_2, \lambda_3)$ on S, the outer boundary of A. Thus, we take as boundary conditions:

$$\partial U/\partial n = (\underline{x} - \underline{\lambda}), \quad \underline{x} \text{ on } S; \tag{3}$$

$$\partial U/\partial n = 0, \quad \underline{x} \text{ on bdry } D. \tag{4}$$

Here, $\delta(\underline{x} - \underline{\lambda})$ is a two-dimensional Dirac delta function and $\partial/\partial n$ denotes the normal derivative directed into A-D. We remark here that this idealized problem applies to a real experiment only in the band limits of the Fourier transform of the time-shape of the source, and then only after normalizing the observed data at each frequency with respect to that source.

We set,

$$U = U_I + U_S \quad , \tag{5}$$

where

$$U_I(\underline{x},\underline{\lambda}) = \frac{\exp\{i\omega|\underline{x} - \underline{\lambda}|/c}{2\pi|\underline{x} - \underline{\lambda}|} \quad . \tag{6}$$

Here, $\underline{x} = (x_1, x_2, x_3)$ denotes any point in D. The function U_I is the probe and the function U_S contains all of the response due to the hole, D, and due to the nature of S.

We shall observe the scattered field at $\underline{\xi} = (\xi_1, \xi_2, \xi_3)$ on S. We assume that, by "time-gating" the observations, the response due to D alone can be identified. Equivalently, we remove the boundary S and take U_S to be the response to the hole D alone due to the source U_I given by Eq. (6).

We introduce the Green's function:

$$g(\underline{x},\underline{\xi}) = 1/2\ U_I(\underline{x},\underline{\xi}) = \frac{\exp\{i\omega|\underline{x} - \underline{\xi}|/c}{4\pi|\underline{x} - \underline{\xi}|} \quad . \tag{7}$$

We can then deduce the following integral representation for the response at $\underline{\xi}$ due to the source at $\underline{\lambda}$ (see, for example, Baker and Copson, 1950):

$$U_S(\underline{\xi},\underline{\lambda}) = \int_S [U_I(\underline{x},\underline{\lambda}) + U_S(\underline{x},\underline{\lambda})] \frac{\partial}{\partial n} g(\underline{x},\underline{\xi}) dS \quad . \tag{8}$$

Similarly, we can deduce that:

$$0 = \int_S [U_I(\underline{x},\underline{\xi}) \frac{\partial}{\partial n} g(\underline{x},\underline{\xi}) - g(\underline{x},\underline{\xi}) \frac{\partial U}{\partial n}(\underline{x},\underline{\lambda})] dS \quad . \tag{8}$$

Similarly, we can deduce that:

$$0 = \int_S [U_I(\underline{x},\underline{\lambda}) \frac{\partial}{\partial n} g(\underline{x},\underline{\xi}) - g(\underline{x},\underline{\xi}) \frac{\partial U}{\partial n}(\underline{x},\underline{\xi})] dS \quad , \tag{9}$$

which we shall use below.

For the small hole size (say, $9(\varepsilon)$), we expect that U_S will be small (also $9(\varepsilon)$), and thus the integral involving U_S in Eq. (8) will be even smaller. Thus we approximate U_S by:

$$U_S(\underline{\xi},\underline{\lambda}) = \int_S U_I(\underline{x},\underline{\lambda}) \frac{\partial g}{\partial n}(\underline{x},\underline{\lambda}) dS \quad . \tag{10}$$

This is the Born approximation.

We now use Eq. (9) to write this result in the more symmetric form:

$$U_s(\underline{\xi},\underline{\lambda}) = \tfrac{1}{4}\int_S [\,U_I(\underline{x},\underline{\lambda})\,\frac{\partial}{\partial n}\,g(\underline{x},\underline{\xi}) + g(\underline{x},\underline{\xi})\,\frac{\partial}{\partial n}\,U_I(\underline{x},\underline{\xi})]\;dS\;, \tag{11}$$

or

$$U_s(\underline{\xi},\underline{\lambda}) = \tfrac{1}{4}\int_S \underline{n}\cdot\nabla[\,U_I(\underline{x},\underline{\lambda})\;g(\underline{x},\underline{\xi})]\,dS\;. \tag{12}$$

By using the divergence theorem here, we find:

$$U_s(\underline{\xi},\underline{\lambda}) = \tfrac{1}{4}\int_D \nabla^2[\,U_I(\underline{x},\underline{\lambda})\;g(\underline{x},\underline{\xi})]\,dV\;. \tag{13}$$

Let us now suppose that we have some appropriate idea of where the flaw is located† and take that location to be $\underline{r}_o$ in or near D. By this latter phrase we mean that:

$$\frac{|\underline{x}-\underline{r}_o|}{|\underline{\lambda}-\underline{r}_o|} \ll 1, \quad \frac{|\underline{x}-\underline{r}_o|}{|\underline{\xi}-\underline{r}_o|} \ll 1, \quad \underline{x}\text{ in D.} \tag{14}$$

These estimates will be used to simplify Eq. (13), in which $\underline{x}$ is in D. To do so, we return to Eq. (6) and rewrite that equation as:

$$U_I(\underline{x},\underline{\lambda}) = \frac{\exp\{i\omega|\underline{\lambda}-\underline{r}_o-(\underline{x}-\underline{r}_o)|/c\}}{2\pi|\underline{\lambda}-\underline{r}_o-(\underline{x}-\underline{r}_o)|}\;. \tag{15}$$

We now apply the binomial theorem in the following form:

$$|\underline{\lambda}-\underline{r}_o-(\underline{x}-\underline{r}_o)| = |\underline{\lambda}-\underline{r}_o| \times\left\{1-\frac{(\underline{\lambda}-\underline{r}_o)\cdot(\underline{x}-\underline{r}_o)}{|\underline{\lambda}-\underline{r}_o|^2} + O\left(\frac{|\underline{x}-\underline{r}_o|}{|\underline{\lambda}-\underline{r}_o|}^2\right)\right\} \tag{16}$$

By using this result in Eq. (15) we conclude that:

$$U_I(\underline{x},\lambda) = \frac{\exp\{i\omega|\underline{\lambda}-\underline{r}_o|/c+i\omega\hat{\lambda}\cdot\underline{y}\}}{2\pi|\underline{\lambda}-\underline{r}_o|} \times\left\{1+O\left(\frac{|\underline{x}-\underline{r}_o|}{|\underline{\lambda}-\underline{r}_o|}\right)\right\} \tag{17}$$

Here, we have introduced the notation:

$$\hat{\lambda} = \frac{\underline{\lambda}-\underline{r}_o}{|\underline{\lambda}-\underline{r}_o|}\;, \quad \underline{y} = \underline{x}-\underline{r}_o\;. \tag{18}$$

Similar approximations can be made in $g(\underline{x},\underline{\xi})$ given by Eq. (7) and for all of the derivatives appearing in Eq. (13). After some algebra, we conclude that:

$$U_s(\underline{\xi},\underline{\lambda}) = \frac{\exp\{i\omega(|\underline{\lambda}-\underline{r}_o|+|\underline{\xi}-\underline{r}_o|)/c\}}{(4\pi^2)|\underline{\lambda}-\underline{r}_o|\;|\underline{\xi}-\underline{r}_o|}\;I(\tfrac{\omega}{c},\hat{\lambda},\hat{\xi}). \tag{19}$$

†Delay time observations would suffice to produce this first approximation of the location of the hole.

Here, we have introduced the variable;

$$\hat{\xi} = \frac{\underline{\xi}-\underline{r}_o}{|\underline{\xi}-\underline{r}_o|}\;, \tag{20}$$

and

$$I(\omega/c,\hat{\lambda},\hat{\xi}) = -[\frac{\omega(\hat{\lambda}+\hat{\xi})}{c}]^2\int_D \exp\{i\omega(\hat{\lambda}+\hat{\xi})\cdot\underline{y}\}dV\;. \tag{21}$$

This function is the phase and range normalized far field scattering amplitude.

In order to interpret this result, we introduce $\Gamma(\underline{y})$, the characteristic function of the domain D, defined by:

$$\Gamma(\underline{y}) = \begin{cases} 1, & \underline{y}\text{ in D} \\ 0, & \underline{y}\text{ not in D} \end{cases}\;. \tag{22}$$

The Fourier transform of $\Gamma(\underline{y})$ is given by:

$$\gamma(\underline{k}) = \int_D \exp\{-i\underline{k}\cdot\underline{y}\}dV\;. \tag{23}$$

We then conclude from Eq. (21) that;

$$I(\omega/c,\hat{\lambda},\hat{\xi}) = -k^2\,(\underline{k}) \qquad \underline{k} = \omega(\hat{\lambda}+\hat{\xi})/c,\;\; k = (\underline{k}\cdot\underline{k})^{1/2}\;. \tag{24}$$

In words, the far field scattering amplitude is proportional to the Fourier transform of the characteristic function of the scatterer. Knowledge of $\gamma(\underline{k})$ for "all" $\underline{k}$ (wideband and all directions of the vector) would provide a full description of the scatterer by Fourier inversion. Clearly, such information is not practically available. Thus, it is necessary to explore the question of extracting information about D from aperture limited - band limited and aspect angle limited - observations of the scattered field. Equivalently, we have reduced the problem to a question in Fourier analysis; namely, what sort of information about a characteristic (non-zero) function can be extracted from aperture limited information about its Fourier transform?

The identity, Eq. (24), has previously been derived under the assumption of high frequency[2-4,6,7,9-12] by using physical optics approximations instead of the Born approximation. This distinction is extremely important. In the present case, we may explore the possibility of extracting information about the scatterer from low frequency observations as well as from high frequency observations. In the earlier work, analysis of Eq. (24) for low frequency would have made no sense at all.

In the following ("Low Frequency Analysis of the Characteristic Function"), the low frequency limit is discussed and the question of high frequency information is addressed under "High Frequency Analysis."

Low Frequency Analysis of the Characteristic Function

For the characteristic function and its Fourier transform defined by Eq. (22) and Eq. (23), we define "low frequency" to mean that:

$$ky << 1, \quad \underline{y} \text{ in } D . \tag{25}$$

We assume that the provided observations of $\gamma(\underline{k})$ are sufficient for us to generate a spherical harmonic expansion of $\gamma(\underline{k})$ at least to the order $Y_{22}(\beta,\alpha)$. Here, we use the notation in Jackson, p. 66,[5] with (β,α) the spherical polar angles of $\underline{k}$. We further assume that sufficient observations are made at frequencies subject to Eq. (25) to allow a two-term power series expansion in k of the coefficients of the spherical harmonic expansion. Thus, while we are considering low frequency band limiting here, we are not considering aperture limiting in this case. The latter is a subject for further research not practicable under the present program.

We shall use spherical harmonic expansions to analyze Eq. (23). We begin, then, with the following spherical harmonic expansion of $\gamma(\underline{k})$:

$$\gamma(\underline{k}) = \sum_{\ell=0}^{\infty} \sum_{m=-\ell}^{\ell} Y_{\ell m}(\beta,\alpha) A_{\ell m}(k) . \tag{26}$$

Here, the coefficients $A_{\ell m}(k)$ are defined by:

$$A_{\ell m}(k) = \int_0^{\pi} d \int_0^{\pi} d\beta \; \gamma(\underline{k}) Y_{\ell m}^*(\beta,\alpha) \sin\beta \tag{27}$$

$$0 \leq |m| \leq \ell < \infty ,$$

with (*) denoting complex conjugate. These coefficients can be derived from our observations of $\gamma(\underline{k})$.

On the right side in Eq. (23), we substitute the spherical harmonic expansion of the exponential function:[5]

$$\exp[-i\underline{k}\cdot\underline{y}] = 4\pi \sum_{\ell=0}^{\infty} (-i)^{\ell} j_{\ell}(ky) \sum_{m=-\ell}^{\ell} Y_{\ell m}^*(\theta,\phi) Y_{\ell m}(\beta,\alpha). \tag{28}$$

Here, (θ,ϕ) are the spherical polar angles of the vector $\underline{y}$, j_ℓ is the spherical Bessel function of of the first kind and order ℓ. We conclude then, that

$$A_{\ell m}(k) = 4\pi(-i)^{\ell} \int_D j_{\ell}(ky) Y_{\ell m}^*(\theta,\phi) dV . \tag{29}$$

$$0 \leq |m| \leq \ell < \infty .$$

We define the coefficients in the power series expansions of Eq. (29) by the equations,

$$A_{\ell m}(k) = \sum_{n=0} k^n A^n_{\ell m}, \quad 0 \leq |m| < \ell < \infty . \tag{30}$$

Below, we shall use only $A^0_{\ell m}$, $0 \leq |m| \leq \ell \leq 2$ and A^2_{00}. We begin with:

$$I^0_{00} = \frac{1}{\sqrt{4\pi}} \int_D dV = \frac{1}{\sqrt{4\pi}} \text{ (Volume of D)} . \tag{31}$$

Here, we have used the fact that $j_0(ky) = 1$ to leading order and $Y_{00} = 1/\sqrt{4\pi}$. We shall continue below to use such facts about Bessel functions and spherical harmonics, without stating those facts explicitly.

From Eq. (31) we see that knowledge of I^0_{00} yields the volume of the hole. We now consider the order one terms in the set of $I^n_{\ell m}$.

$$\begin{aligned} A^0_{1,1} + A^0_{1,-1} &= -i\sqrt{8\pi/3} \int_D y_1 dV ; \\ A^0_{1,1} - A^0_{1,-1} &= \sqrt{8\pi/3} \int_D y_2 dV ; \\ A^0_{10} &= -i\sqrt{4\pi/3} \int_D y_3 dV . \end{aligned} \tag{32}$$

Thus, to leading order, the spherical harmonic coefficients of order (1, ±1) and (1, 0) provide the components of the centroid of the domain D. With reference to the observation of the preceding section, these coefficients provide a correction to the approximation $\underline{r}_0$ in Fig. 1.

We now consider all coefficients of order k^2.

$$\begin{aligned} A^2_{00} &= -\frac{2\pi}{3}(I_{11} + I_{22} + I_{33}) \\ A^0_{20} &= -\frac{1}{3}\sqrt{\pi/5}\, I_{33} + \frac{2}{3}\sqrt{\pi/5}\,(I_{11} + I_{22}) \\ A^0_{2,\pm1} &= \sqrt{2\pi/15}\,(I_{13} \pm i\, I_{23}) \\ A^0_{2,\pm2} &= \sqrt{2\pi/15}\,[I_{12} \pm \tfrac{i}{2}(I_{11} - I_{22})] \end{aligned} \tag{33}$$

Here

$$I_{pq} = \int_D y_p y_q dV, \quad p,q = 1,2,3 . \tag{34}$$

These coefficients are the products of inertia (more precisely, because of the lack of a mass density, these are "normalized" products of inertia) of the domain D with respect to the origin, $\underline{r}_0$, of the $\underline{y}$ coordinate system. Before discussing their significance, we remark that they can be determined by inverting the system (Eq. (33)). The result is:

$$\begin{aligned} I_{11} &= \tfrac{1}{2}\{\sqrt{15/2\pi}\,(A^0_{2,2} - A^0_{2,-2}) - \frac{A^2_{00}}{2\pi} + \sqrt{5/\pi}\; A^0_{20}\} ; \\ I_{22} &= \tfrac{1}{2}\{\sqrt{15/2\pi}(A^0_{2,2} - A^0_{2,-2}) - \frac{A^2_{00}}{2\pi} + \sqrt{5/\pi}\; A^0_{24}\} ; \\ I_{33} &= -\frac{A^2_{00}}{\pi} - \sqrt{5/\pi}\, A^0_{20} ; \\ I_{12} &= \sqrt{15/8\pi}\,\{A^0_{2,2} + A^0_{2,-2}\} ; \\ I_{13} &= \sqrt{15/8\pi}\,\{A^0_{2,1} + A^0_{2,-1}\} ; \\ I_{23} &= -i\,\sqrt{15/8\pi}\,\{A^0_{2,1} - A^0_{2,-1}\} . \end{aligned} \tag{35}$$

We shall now transform these products of inertia to a center of mass coordinate system. To do so, let us define the components of the centroid determined in Eq. (32) to be:

$$\bar{y}_p = \int_D y_p dV, \quad p = 1,2,3 . \tag{36}$$

We then define the products of inertia with respect to the centroid coordinate system to be:

$$J_{pq} = \int_D (y_p - \bar{y}_p)(y_q - \bar{y}_q)dV = Y_{pq} - \bar{y}_p\bar{y}_q, \tag{37}$$

$$p,2 = 1,2,3 .$$

To understand the significance of these functions, let us consider the case in which D is an ellipsoid with semi-axes of length, a,b,c, along the coordinate axes. Then the matrix of coefficients (J_{pq}) is diagonal with elements, a^2,b^2,c^2. For any other matrix (J_{pq}), let U be the orthogonal matrix which diagonalizes it. Then U^T, the transpose of U, is the matrix which transforms the coordinate system to principal axes. The diagonal elements of $U^T(J_{pq})U$ then provide the squares of the semiaxes of an equivalent ellipsoid, having the same centroid and products of inertia. Thus, from (J_{pq}) we are able to determine orientation and aspect ratio parameters for D.

High Frequency Analysis

We now address ourselves to the question of extracting information about the size and shape of the domain, D, from knowledge of $\gamma(\underline{k})$ defined by Eq. (23) only for high frequency. Here, by "high frequency" we mean that,

$$ky >> 1, \quad \underline{y} \text{ in } D . \tag{38}$$

As noted under "Basic Formulation," there is a more extensive literature on this problem. We shall outline the results of that analysis and demonstrate the results with computer graphics.

In the high frequency regime it has proven more desirable to process data for a first derivative of $\Gamma(y)$, rather than for $\Gamma(\underline{y})$ itself. When $\Gamma(\underline{y})$ is a characteristic function, the first derivative, $\partial\Gamma/\partial y_1$, for example, is proportional to a Dirac delta function. The proportionality factor is linear in the cosine of the angle between the normal and tye y_1 axis.* We note that,

$$\partial\Gamma/\partial y_1 = 1/(2\pi)^3 \int ik_1\gamma(\underline{k}) \exp i(\underline{k}\cdot\underline{y})dk^3 , \tag{39}$$

with the domain of integration being all of $\underline{k}$ space. Let us suppose that $\gamma(\underline{k})$ is known for all angles of $\underline{k}$, but only for $k_{MIN} < k < k_{MAX}$, with Eq. (38) true for k_{MIN}. This is the case of band-limited (but not aspect angle limited) data.

*For surface elements where cosine is near zero, one could use a derivative with respect to y_2 or y_3.

We denote this annular region in $\underline{k}$-space by B. We set $\gamma(\underline{k})$ equal to zero outside of B and define the band-limited derivative:

$$\partial\Gamma_B/\partial y_1 = 1/(2\pi)^3 \int_B ik_1\gamma(\underline{k}) \exp i(\underline{k}\cdot\underline{y})dk^3 . \tag{40}$$

It has been shown by Mager and Bleistein[7] that, asymptotically, this function is proportional to the so-called "sin k function,"

$$\sin k(r) = \frac{\sin k_{MAX}r}{r} - \frac{\sin k_{MIN}r}{r} , \tag{41}$$

with r measuring minimum distance to the boundary of D. This function "peaks" at r = 0, thus distinguishing the boundary as an envelope of peaks.

We demonstrate the utility of this method through a series of pictorial examples beginning with Fig. 2. The examples are two-dimensional with D being an ellipse having semi-major axis of length, 2, semi-minor axis of length, 1. The Fourier transform of $\Gamma(\underline{k})$ is calculated by fast Fourier transform (FFT). The band limited inverse transform is then calculated using Eq. (40). The result is graphed (in Fig. 2, for example) with the third dimension (the function value) laid back down on the plane. On each line the height is normalized with respect to maximum height. Furthermore, the maximum on each line is tested against the absolute maximum. When this relative maximum falls below a critical value, the entire line is zeroed out. This insures, for example, that "noise" will not be enhanced outside of the vertical extent of the ellipse.

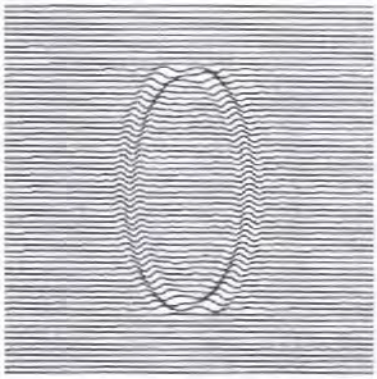

K Range 9-27

Figure 2. High frequency full aperture backscatter reconstruction.

Figure 2 depicts the result of very high frequency bandwidth processing, $9 \leq k \leq 27$. The characteristic main lobe-side lobe pair of the sin k function are observed on each line. The narrowness of the main lobe is a consequence of the high frequencies used. The relative height of the side lobes is a consequence of the percentage bandwidth,

$$\frac{k_{MAX} - k_{MIN}}{k_{MAX} + k_{MIN}} \times 100 ,$$

that was used here; namely 50%. This main lobe-side lobe configuration provides a characteristic signature. At this bandwidth, all further side lobes are virtually nil.

Figures 3 and 4 depict the results for lower frequency ranges 6 to 18 and 3 to 9, respectively, but the same 50% bandwidth. In Fig. 4, it is clear that visualization is becoming difficult. However, resolution can be improved by "curve fitting" the data to the known sin k function on each line. In Fig. 5, we repeat the frequency range of Fig. 4, but add the reference zero line at each level. The main lobe and two side lobes appear here as a characteristic triple of dark bands separated by two light bands produced by the zero crossings of the sin k function. The increased coherence in the picture is suggestive of the potential for analytical resolution enhancement. Figure 6 demonstrates the complete breakdown of this method when low to moderate frequency data is employed. We remark, however, that size and orientation are suggested by the figure, consistent with the conclusions of the discussion on "Low Frequency Analysis of the Characteristic Function."

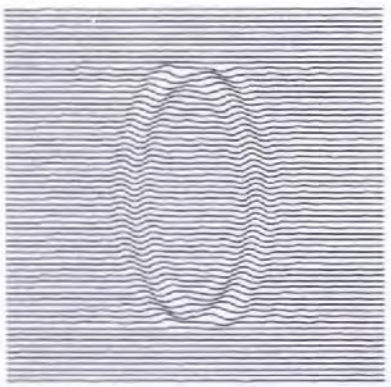

K Range 6-18

Figure 3. Medium high frequency full aperture backscatter reconstruction.

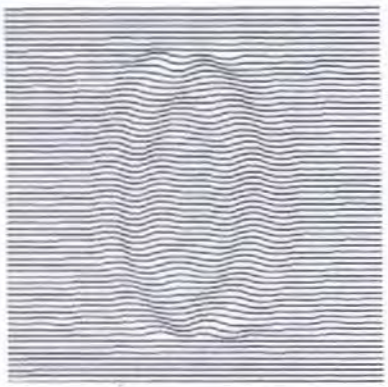

K Range 3-9

Figure 4. Medium frequency full aperture backscatter reconstruction.

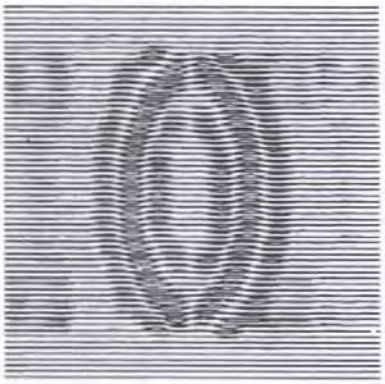

K Range 3-9

Figure 5. Medium frequency full aperture backscatter reconstruction and zero reference lines.

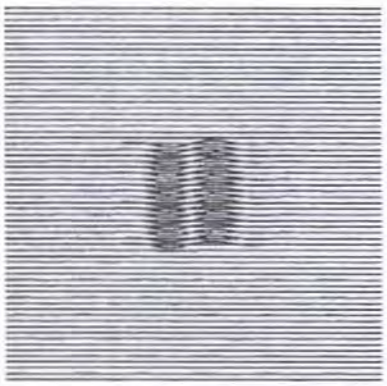

K Range .4-2.4

Figure 6. Low frequency full aperture backscatter reconstruction.

In Mager and Bleistein,[7] the problem of aspect limiting was considered as well. We showed that an angular aperture in $\underline{k}$-space defined an angular aperture in physical space in which the results were the same as for the full angular aperture case discussed above. The angular aperture in physical space is that one in which the normal direction of the boundary of D lies in the angular aperture in $\underline{k}$-space. Figures 7 and 8 demonstrate results for two symmetric 90° apertures. (Symmetric apertures are chosen for examples for convenience. They are not necessary for the theory.) In Fig. 8, considerable "spill-over" outside the predicted aperture is observed. This is well understood and discussed in the above cited paper.

Figure 7. High frequency limited aperture reconstruction.

Figure 8. Medium frequency limited aperture reconstruction.

In all of these examples, we have only demonstrated the extraction of information from an aperture limited (band limited and aspect angle limited) Fourier transform. In Mager and Bleistein,[7] the identity, Eq. (24), itself was verified in the high frequency case. This was done by determining I in the backscatter case, $\hat{\lambda} = \hat{\xi}$, by solving the scattering problem for a sphere numerically. The data was then phase and range normalized at 25 radii to produce I. We include one aperture limited diagram from that paper in Fig. 9. In that paper, we also showed that the same results will be obtained in three dimensions.

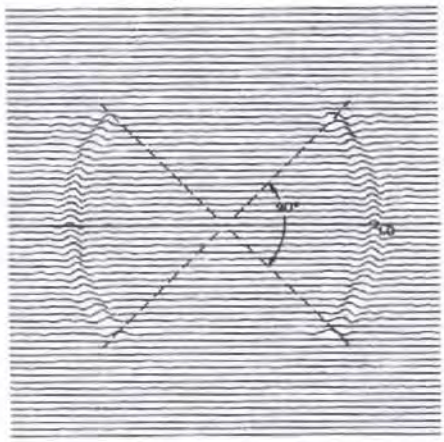

Figure 9. Limited aperture reconstruction from backscattered data at 25 radii.

Acknowledgement

This research was sponsored by the Center for Advanced NDE operated by the Science Center, Rockwell International, for the Advanced Research Projects Agency and the Air Force Materials Laboratory under contract F33615-74-C-5180.

References

1. B. B. Baker and E. T. Copson, The Mathematical Theory of Huygens Principle, 2nd Ed., Oxford (1950).

2. N. Bleistein, "Direct Image Reconstruction of Anomalies in a Plane via Physical Optics Forefield Inverse Scattering," J. Acous. Soc. Am., 59, 6, 1259-1264 (1976).

3. N. Bleistein, "Physical Optics Far Field Inverse Scattering in the Time Domain, J. Ac. Soc. Amer., 60, 6, 1249-1255 (1977).

4. N. N. Bojarski, "Three-Dimensional Electromagnetic Shortpulse Inverse Scattering," Syracuse University Research Corporation, Syracuse, New York (1967).

5. J. D. Jackson, Classical Dynamics, Wiley, New York (1962).

6. R. M. Lewis, "Physical Optics Inverse Diffraction," IEEE Trans. Ant. Prop. AP-17, 308-314 (1969).

7. R. Mager and N. Bleistein, "An Approach to the Limited Aperture Problem of Physical Optics Farfield Inverse Scattering," Denver Research Institute Report #MS-R-7704 (1976).

8. P. M. Morse, and Feshback, Methods of Theoretical Physics, McGraw-Hill, New York (1953).

9. W. L. Perry, "On the Bojarski-Lewis Inverse Scattering Method," IEEE Trans. Ant. Prop., Ap-22, 6, 826-829 (1974).

10. S. Rosenbaum-Raz, "On Scatterer Reconstruction from Farfield Data," IEEE Trans. Ant. Prop., AP-24, 66-70 (1976).

11. W. Tabbara, "On an Inverse Scattering Method," IEEE Trans. Ant. Prop., AP-21, 245-247 (1973).

12. W. Tabbara, "On the Feasibility of an Inverse Scattering Method," IEEE Trans. Ant. Prop., AP-23, 446-448 (1975).